PL/PA 5/15/97

NUMERICAL ANALYSIS OF A TRANSMISSION LINE EMP SIMULATOR

Keith M. Soo Hoo
The Aerospace Corporation

ABSTRACT

A theoretical model is defined for an electromagnetic pulse (EMP) simulator for testing EMP effects on high altitude satellites. The simulator is composed of three flat-plate transmission line sections. The first and third sections are tapered to accommodate, respectively, a generator and a terminating resistor. This problem is analyzed in the frequency domain over those frequency components which are known to contribute most significantly to a typical EMP waveform.

The analysis uses a numerical technique to solve the basic problem of an unknown current distribution on a curved, tapered strip, excited by a known electric field. The unknown current is solved by the method of moments, using triangular basis functions. To check the computer program, input impedances are computed for the triangular dipole. It is shown that these solutions compare quite favorably with experimental results. Variations in the solutions are also demonstrated for these same cases when edge singularities are not taken into account in the analysis.

For the transmission line simulator, computed input impedance, VSWR, power dissipated in the terminating resistor, and the power lost to radiation are presented as a function of frequency. The computed current distributions are used

PL 96-1002

to calculate the electric fields between and immediately beyond the parallel plates. Although a considerable portion of power is converted to radiation at the higher frequencies, it is shown that at least within the working volume the eletric field maintains a reasonably constant level.

CONTENTS

FIGURES

TABLE

I. INTRODUCTION

Static field analysis has shown that the TEM mode of a parallel plate transmission line can simulate a free-space plane electromagnetic wave over a substantial portion of its interior region (Ref. 1). This method, however, does not account for the presence of higher order modes which may exist whenever the plate separation exceeds half a wavelength. For this case a dynamic field solution would be necessary. A high altitude EMP waveform consists of frequency components in the HF-VHF regime. Many wavelengths may therefore exist between the parallel plates of a transmission line designed to accommodate EMP testing of missiles or satellites.

This paper considers the dynamic field analysis of a high altitude EMP simulator. The simulator consists of a parallel plate transmission line that is tapered at both ends to accommodate a generator and a terminating load. The analysis is performed in the frequency domain, using the method of moments (Ref. 2).

This numerical technique has the overriding advantage that the current everywhere on the transmission line can be accurately computed. It is then reasonably straightforward to obtain all of the quantities of interest (e.g., the electromagnetic fields both interior and exterior to the transmission line, the input impedance, the power absorbed by the terminal load, and the power lost to radiation). The principal disadvantage is that the method of moments cannot be applied to structures whose dimensions are considerably larger than a wavelength. This limitation is dependent on the storage capacity and running costs of the particular computer being used.

For the purpose of the analysis, the basic element of the simulator is a tapered conducting strip. The numerical analysis of flat strips and rectangular plates has been considered previously (Refs. 3, 4), and the tapered strip may be treated in generally the same manner. At the outset one should allow for two-dimensional variations for the unknown current density vector.

However, this would lead to a system of two integral equations whose solution would be practical only at the extremely low end of the frequency band. In the discussion to follow, it is shown how the frequency range can be extended by making some a priori assumptions on the form of the unknown current. These important assumptions are checked by considering some special test cases for which there exists experimental data.

II. THE GEOMETRY

The simulator geometry relative to a cartesian coordinate system is shown in Fig. 1. In the "working volume" (i.e., the region in which the test object is usually placed) the two plates are of width W_H and are separated by a distance H. Outside of the working volume the plates are tapered down to where they can be made both physically and electrically compatible with the voltage source and the terminal load. For this study, both the source and the load are assumed to be uniformly distributed across the gaps at $x = -(R + D/2)$ and $x = +(R + D/2)$ respectively.
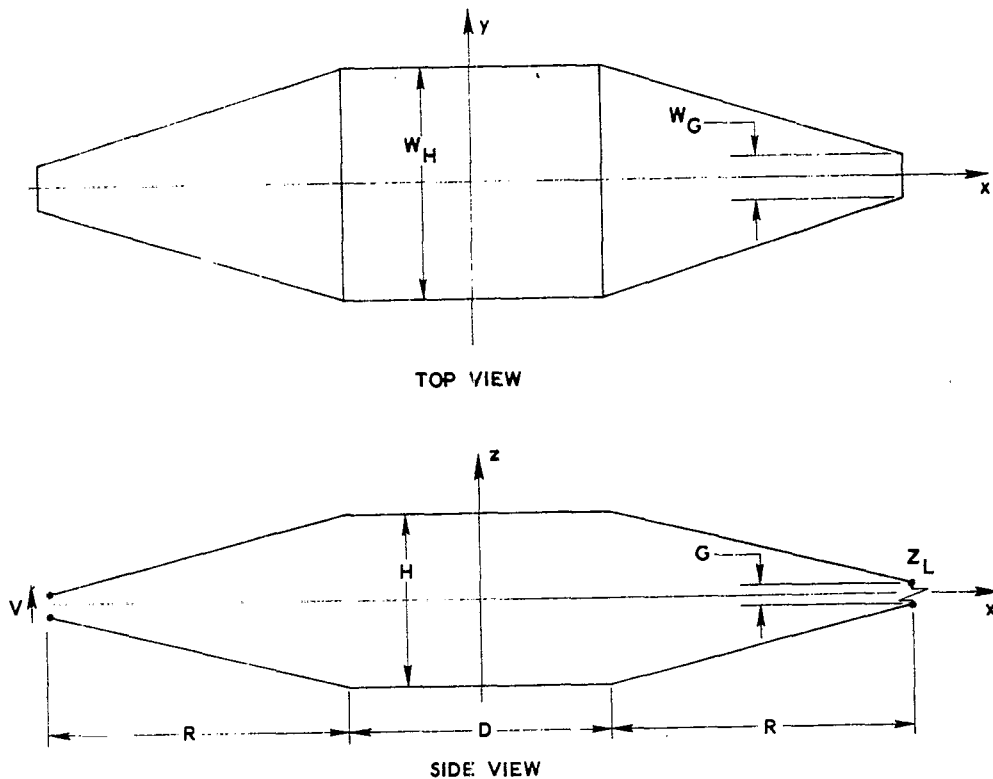
TOP VIEW

SIDE VIEW

Fig. 1. Transmission Line Simulator Geometry

III. THEORY

Let S be the surface defined by the conducting plates and the non-conducting source and terminal gaps of the transmission line. Then one can obtain the following integral equation for the unknown current density J:

$$-j\omega\mu_o \iint_S \vec{J}(\vec{r'})\,\phi\,dS'' + \frac{\nabla_t}{j\omega\epsilon_o} \iint_S \nabla'_t \cdot \vec{J}(\vec{r'})\,\phi\,dS'$$

$$= -\vec{E}^i_{tan} + Z_s(\vec{r})\,\vec{J}, \text{ on S} \qquad (1)$$

where

$$\phi = \frac{1}{4\pi}\,\frac{e^{-jk|\vec{r}-\vec{r'}|}}{|\vec{r}-\vec{r'}|} \qquad (2)$$

Eq. (1) is known as the electric field integral equation and stems from the boundary conditions on the total electric field. Its derivation is given elsewhere (Ref. 5). In Eqs. (1) and (2), $\vec{r}$ and $\vec{r'}$ are vectors from the origin to the source and field points, respectively. Also, $\vec{E}^i_{tan}$ is the tangential component of the incident (or excitation) electric field, which is zero everywhere on S except across the source gap, where it is assumed known. The load impedance Z_s is for a unit length and unit width and is nonzero only across the terminal gap. Finally, ∇_t is the gradient operator in the direction tangent to S, and $k = \omega(\mu_o\epsilon_o)^{1/2}$ is the free-space wave number.

The induced current actually resides on both sides of S. However, because of the assumption that S is infinitesimally thin, Eq. (1) correctly involves only $\vec{J}$, which is the sum of the currents on both sides, and the

8

integration is performed over only one side of S. The current density is next expanded in a set of basis functions $\vec{J}_n$ (to be defined later) as follows:

$$\vec{J} = \sum_{n=1}^{N} I_n \vec{J}_n \qquad (3)$$

where N represents the number of subintervals to be defined later.

If the inner product of Eq. (1) is taken with $\vec{J}_m$, Eq. (1) may be transformed into a set of algebraic equations given by

$$\left[Z_{mn} + Z_{L_{mn}} \right] \left[I_n \right] = \left[V_m \right] \qquad (4)$$

where

$$V_m = \iint_S \vec{J}_m \cdot \vec{E}_{tan}^i \, dS \qquad (5)$$

$$Z_{mn} = j\omega\mu_o \iiiint_{S \ S} \left[\vec{J}_m(\vec{r}) \cdot \vec{J}_n(\vec{r}') - \frac{1}{k^2} (\nabla_t \cdot \vec{J}_m)(\nabla_t' \cdot \vec{J}_n) \right] \phi \, dS' \, dS \qquad (6)$$

$[Z_{mn}]$, $[I_n]$, and $[V_m]$ are the generalized impedance, current, and voltage matrices, respectively, and $[Z_{L_{mn}}]$ is a matrix determined by the terminal load. Again, the detailed steps leading to Eq. (4) are well documented (Ref. 5). This technique is known as Galerkin's method and is a special case of the method of moments.

Eq. (4) may be solved on a computer using a standard matrix inversion algorithm. Once $[I_n]$ has been determined, the problem is essentially solved. However, we need to investigate more fully the determination of $[Z_{mn}]$, since this is the most difficult portion of the calculation.

The first step is to define the basis function $\vec{J}_n$. It is convenient to describe S parametrically in terms of a single variable t. According to Fig. 1, the projection of S onto the x-z plane may be represented by the curve $x = x(t)$ and $z = z(t)$. If W is defined as the width of S, then W may also be expressed as a function of t. These three parametric expressions, which describe S uniquely, may be easily derived in terms of the dimensions of the simulator and are given in the Appendix. Both the starting and ending points ($t = 0$ and $t = L$, respectively) have been arbitrarily set at ($x = -R - D/2$, $z = 0$). The total arc length L is also given in the Appendix.

The basis function may then be expressed in terms of t and the cartesian coordinate y. The basis function should be relatively simple, so as to make the calculation of Z_{mn} as tractable as possible, but it should also provide a reasonable approximation to the current. It is assumed to be of the following form:

$$\vec{J}_n(t, y) = \frac{T_n(t) \ V(t, y)}{W(t)} \ \vec{u}(t, y) \tag{7}$$

T_n is the triangular pulse function used by Harrington and Mautz (Ref. 5), and

$$V(t, y) = \left(1 - \frac{2y}{W}\right)^{-1/2} + \left(1 + \frac{2y}{W}\right)^{-1/2} \tag{8}$$

$$\vec{u}(t, y) = \frac{W\vec{u}_t + yW'\vec{u}_y}{\sqrt{W^2 + (yW')^2}} \tag{9}$$

where $\vec{u}_t$ and $\vec{u}_y$ are unit vectors along the t and y directions respectively ($\vec{u}_t$ is a function of t, and its parametric representation is given in the Appendix).

The triangular function provides a piecewise linear approximation to variations of the current with t. The function $V(t, y)$ is integrably singular at the edges of S ($y = \pm W/2$), and the Sommerfeld edge condition is satisfied by this assumption (Ref. 6). The unit vector $\vec{u}$ has been selected such that the basis function is directed along the edge of S at the edge and along the center line at $y = 0$ and is linearly distributed in between.

To recapitulate, the basis function has been selected such that variations of the current in the transverse direction (y) are specified, variations in the longitudinal direction (t) will be determined in a piecewise linear sense by solving Eq. (4) for $[I_n]$, and the direction of the current is also specified. Obviously we have not started with the most general basis function. But the assumed function provides for greater than a factor of 2 reduction in N, the size of $[Z_{mn}]$, and therefore represents a significant savings in computer storage and computation time. Substitution of Eqs. (7) - (9) into (6) gives

$$Z_{mn} = \frac{j\omega\mu_o}{2} \int_0^L \int_0^L \int_{-W/2}^{W/2} \int_{-W/2}^{W/2} K(t, y)\, K(t', y') \left\{ T_m(t)\, T_n(t') \right.$$

$$(10)$$

$$\times \left[\vec{u}_t \cdot \vec{u}_{t'} + \frac{yy'W''(t)\, W''(t')}{W(t)\, W(t')} \right] - \frac{1}{k^2} T_m'(t)\, T_n'(t') \right\} \phi\, dy\, dy'\, dt\, dt'$$

where

$$K(t, y) = \frac{1}{2} V(t, y) \left[W^2 + (yW')^2 \right]^{-1/2} \qquad (11)$$

The integrations over y and y' may be performed numerically. The integrations over t and t' may be handled in the same manner as shown by Harrington and Mautz (Ref. 5). Thus, further details will not be given here.

The generalized voltage matrix defined by Eq. (5) is quite easy to calculate. From the previous discussion it should be clear that there is a one-to-one correspondence between the subscripts m or n and the triangular pulse function. When m, n = 1 we shall center the triangular function at t = L/N; when m, n = 2 we shall center the triangular function at 2L/N, etc.; then if it is assumed that a 1-volt source is applied across the feed gap

$$[V_m] = \begin{bmatrix} 0 \\ \vdots \\ \vdots \\ 0 \\ 1 \end{bmatrix} \tag{12}$$

The above matrix was derived assuming that the gap height G is infinitesimally small, so that $\vec{E}_{tan}^i$ is a delta function. For the dimensions of interest, this approximation is quite reasonable.

Using the same previous arguments, the matrix $\left[Z_{L_{mn}}\right]$ is also easy to derive. Since the terminal load is located at t = L/2, one gets

$$\left[Z_{L_{mn}}\right] = \begin{bmatrix} 0 & . & . & . & 0 \\ & \ddots & & & \\ & & 0 & & \\ . & & Z_L & & . \\ & & & 0 & \\ . & & & \ddots & . \\ 0 & . & . & . & 0 \end{bmatrix} \tag{13}$$

Once $[I_n]$ has been determined from Eq. (4) the electromagnetic fields may be computed. If the field point is far away (many wavelengths) from the simulator, the current may be approximated by N discrete sources whose amplitudes are I_n, and the field calculation is quite simple. If the field point is near or within the simulator the piecewise linear approximation must be

retained, and an integration over S must be performed. The integration may be approximated in the same manner that Eq. (10) was approximated, and the details will not be presented here.

We include one final word on $[Z_{mn}]$. Since the simulator is symmetric about both the z = 0 and x = 0 planes, it should not be necessary to compute all of the elements of $[Z_{mn}]$. This is illustrated in Fig. 2. Only the matrix elements in the shaded area need to be calculated. It can be proven that A, B, C, and D are axes of symmetry (D is an axis of symmetry because of reciprocity). Therefore all matrix elements in the unshaded region may be generated by making four successive mathematical reflections about A, B, C, and D. This results in a significant reduction in computer time.
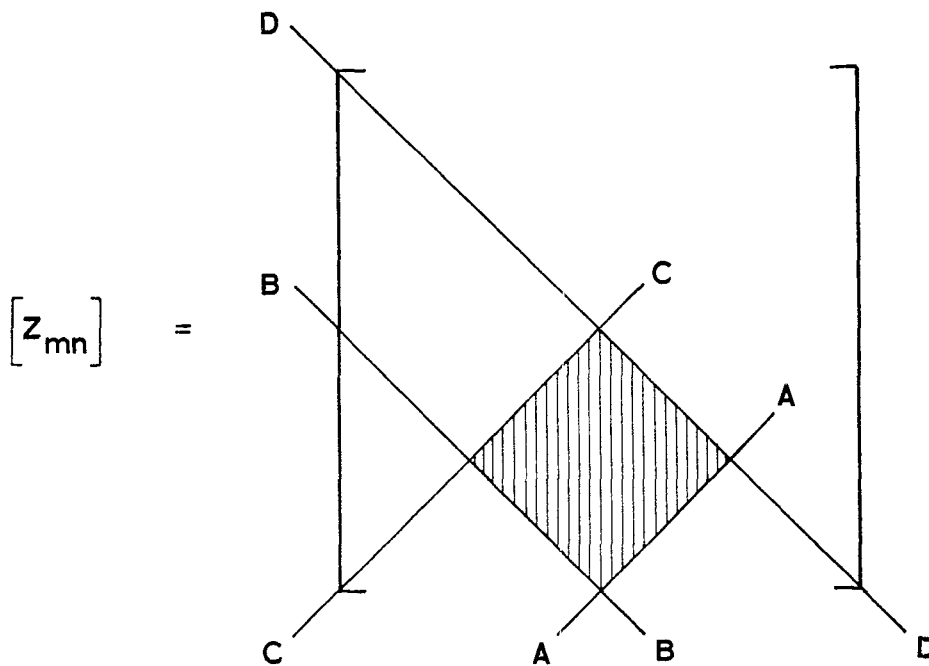

Fig. 2. Symmetry Axes in Generalized Impedance Matrix

13

IV. RESULTS

Calculations were first made on a triangular dipole antenna (i.e., a center-fed symmetric dipole whose radiating arms are triangular plates), since these results can be compared with existing experimental data (Ref. 7) The calculated and measured input impedances are shown in Fig. 3. Representation I is the calculated result using the theory presented in Section III. It can be seen that agreement with experiment is excellent.

Representation II is the result of using a simplified basis function. For this case the basis function was assumed to be uniform in the transverse direction, and in each subinterval the width of S was assumed to be constant. Thus instead of Eqs. (8) and (9) we now have $V(t, y) = 1$ and $\vec{u}(t, y) = \vec{u}_t$. Representation II, although inferior to Representation I, gives reasonably good agreement with the experimental results. Thus Representation II may be used whenever it is considered desirable to trade off accuracy with more favorable computer costs. Most of the calculations on the simulator used Representation II.
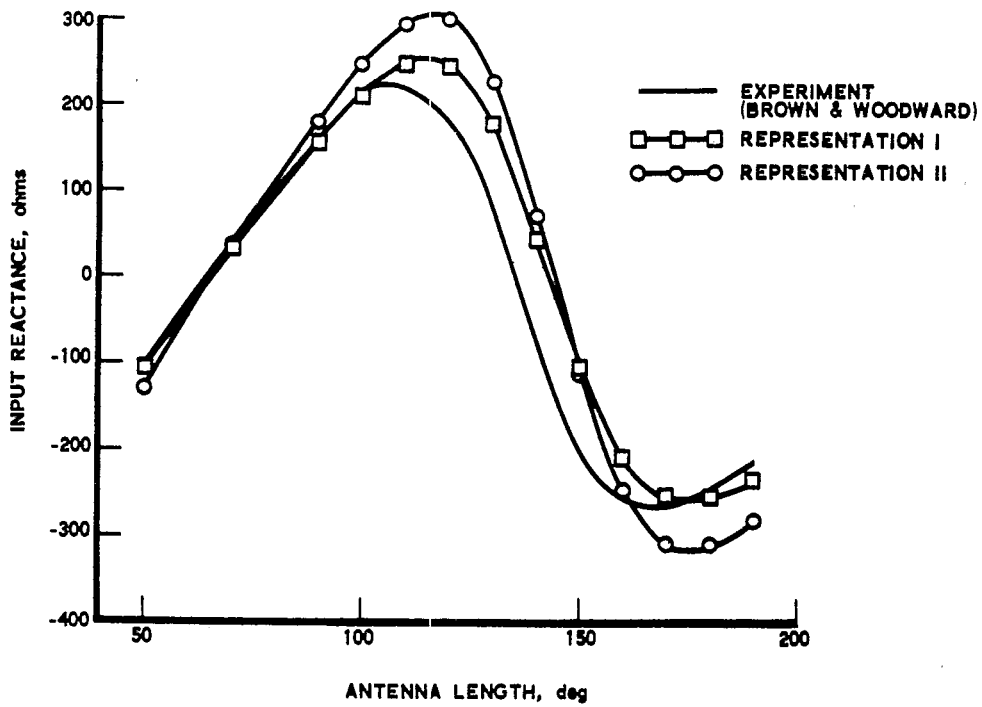
For this study a single set of dimensions was selected (Table I). The feed (terminal) gap was designed such that the characteristic impedance at the input (output) is 100 Ω according to the formula $Z_o = (\mu_o/\epsilon_o)^{1/2} G/W_G$.

Table I. Simulator Dimensions

$$
\begin{array}{lll}
H & = & 12 \text{ m} \\
G & = & 0.2 \text{ m} \\
W_H & = & 18 \text{ m} \\
W_G & = & 0.754 \text{ m} \\
R & = & 20 \text{ m} \\
D & = & 18 \text{ m}
\end{array}
$$
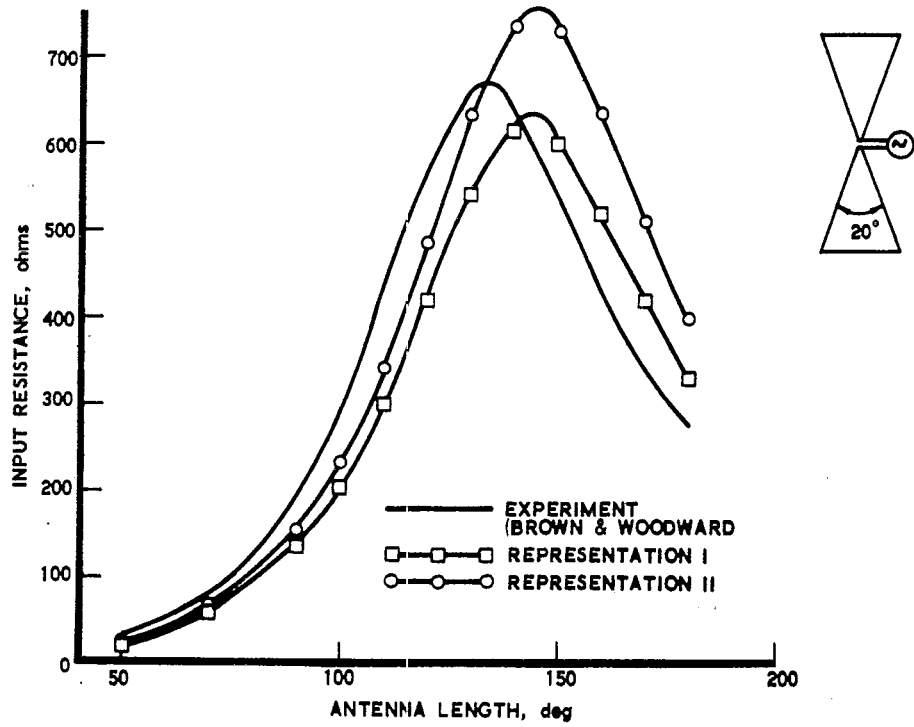
Fig. 3. Input Resistance (a) and Input Reactance (b)
of Triangular Dipole Antenna

For the set of dimensions given in Table I, the total arc length L is 119.81 m. Calculations were performed for frequencies ranging from 2 to 30 MHz. It was found that sufficient accuracy can be obtained for the parameters of interest (most of which are near field parameters) when the subinterval size is less than one-eighth of a wavelength. Therefore the number of subintervals N was chosen to be 40 at the lower frequencies and was increased to 100 at the higher frequencies.

Computed total currents as a function of t are shown in Figs. 4 and 5. The total current is defined by

$$I(t) = \int_{-W/2}^{W/2} \vec{J}(t) \cdot \vec{u}(t, y) \, dy \qquad (14)$$

These values result from a 1-volt source applied across the feed gap. The current on the bottom plate is equal in value, but opposite in direction, and is therefore not shown. The load impedance Z_L for all cases was 100 Ω. It can be seen that the current decays with distance from the feed gap and that the decay is faster at the higher frequency. This suggests that energy may be leaking away through radiation.

The input-resistance and input reactance are shown as a function of frequency in Figs. 6 and 7 respectively. Since a perfectly matched line would have zero reactance, and the input resistance and the characteristic impedance of the line would be equal, it is possible that 100 Ω is not the optimum load. However, as shown in Fig. 8, the impedance mismatch is minimal. It can be seen that the maximum VSWR (relative to 100 Ω) is 1.8, but that mostly it is below 1.5, which corresponds to a power reflection coefficient of less than 0.06. Also shown in Fig. 8 is the percent of incident power being radiated. This is easily determined from the input current and the current at the load. It can be seen that a large amount of power is radiated at the higher frequencies, which is consistent with the current decay shown previously.
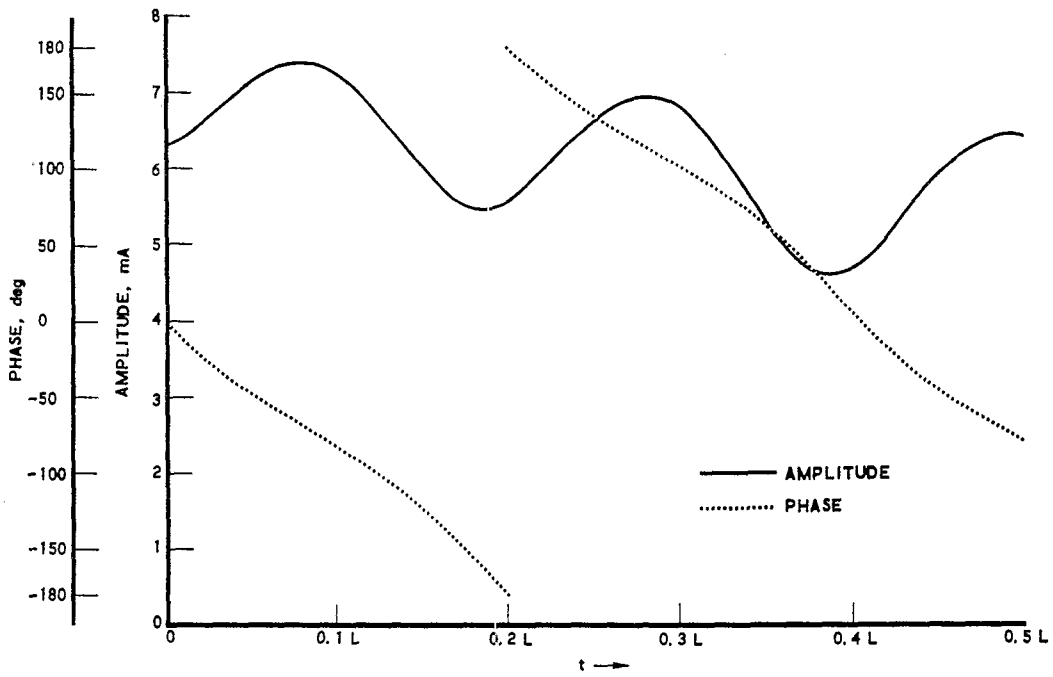
16

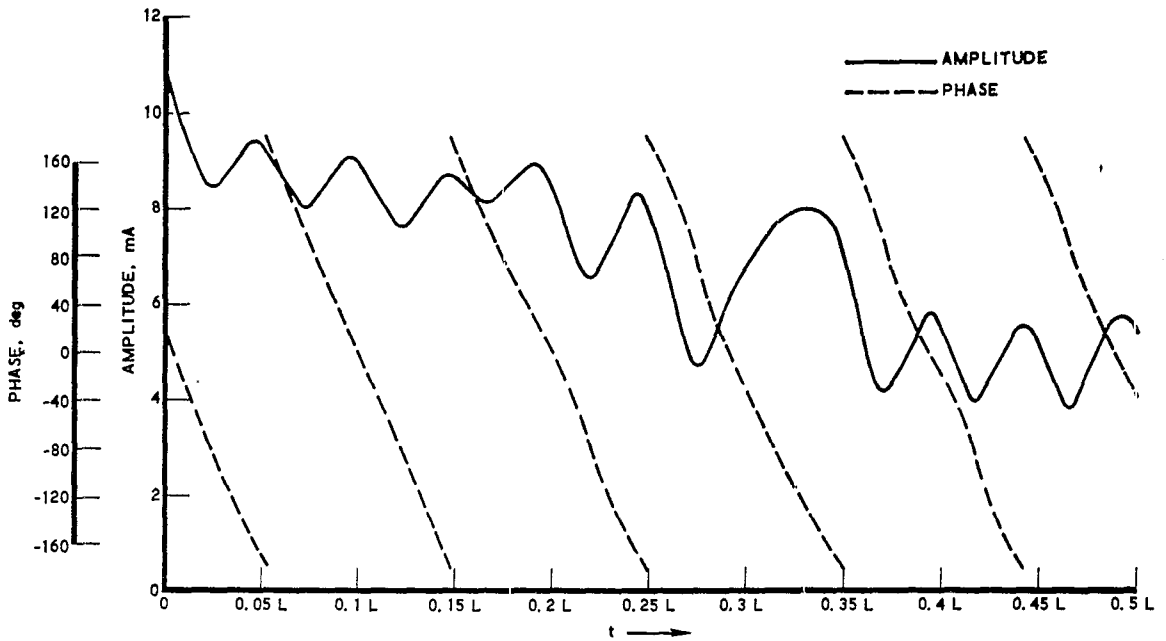Fig. 4.   Current Distribution at 6 MHz
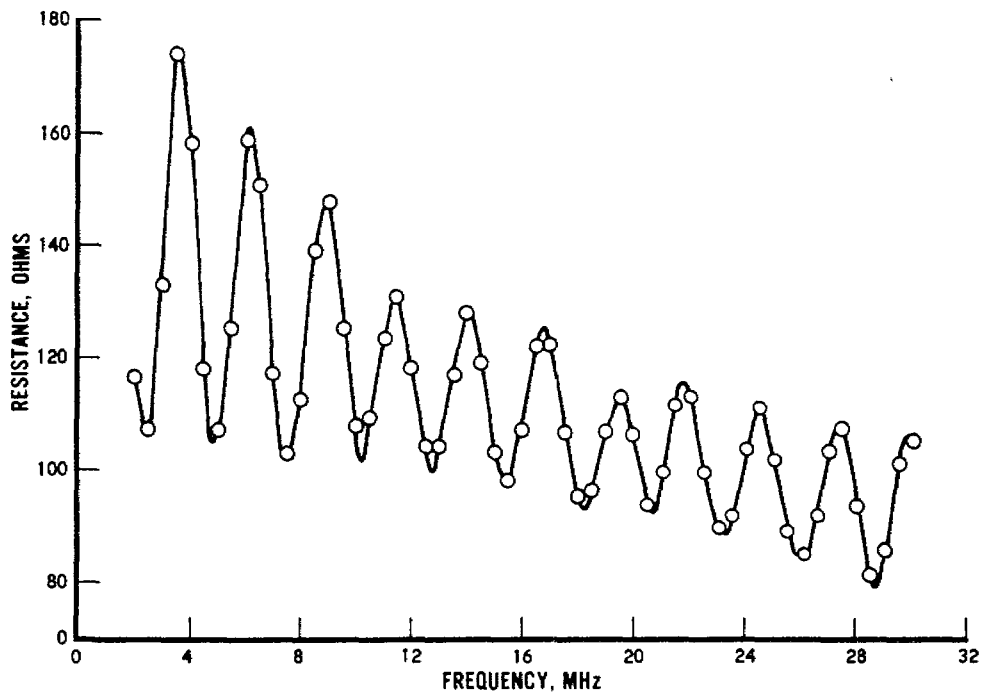

Fig. 5.   Current Distribution at 26 MHz

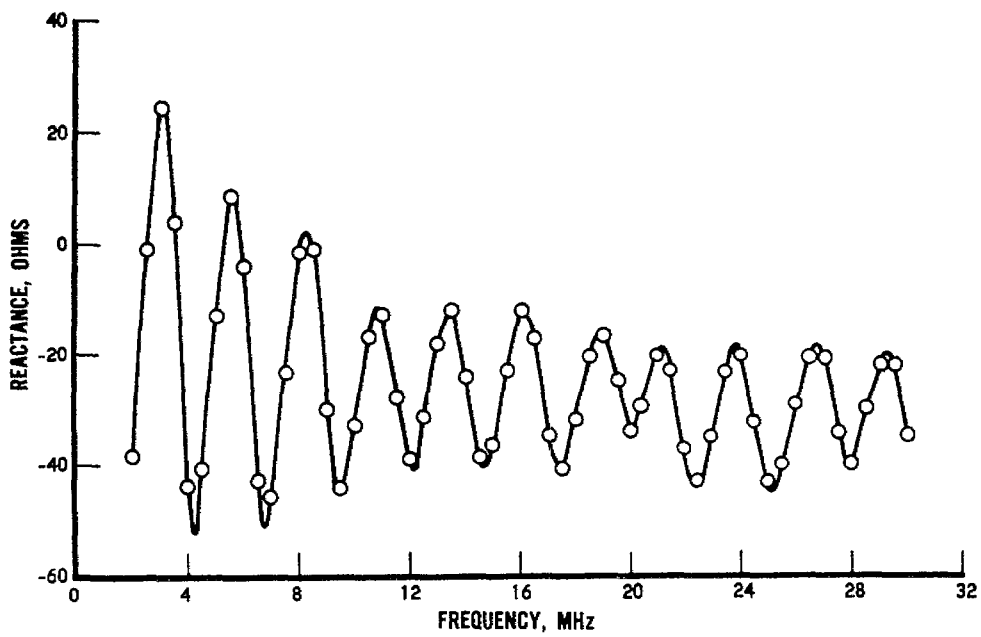Fig. 6. Input Resistance vs Frequency

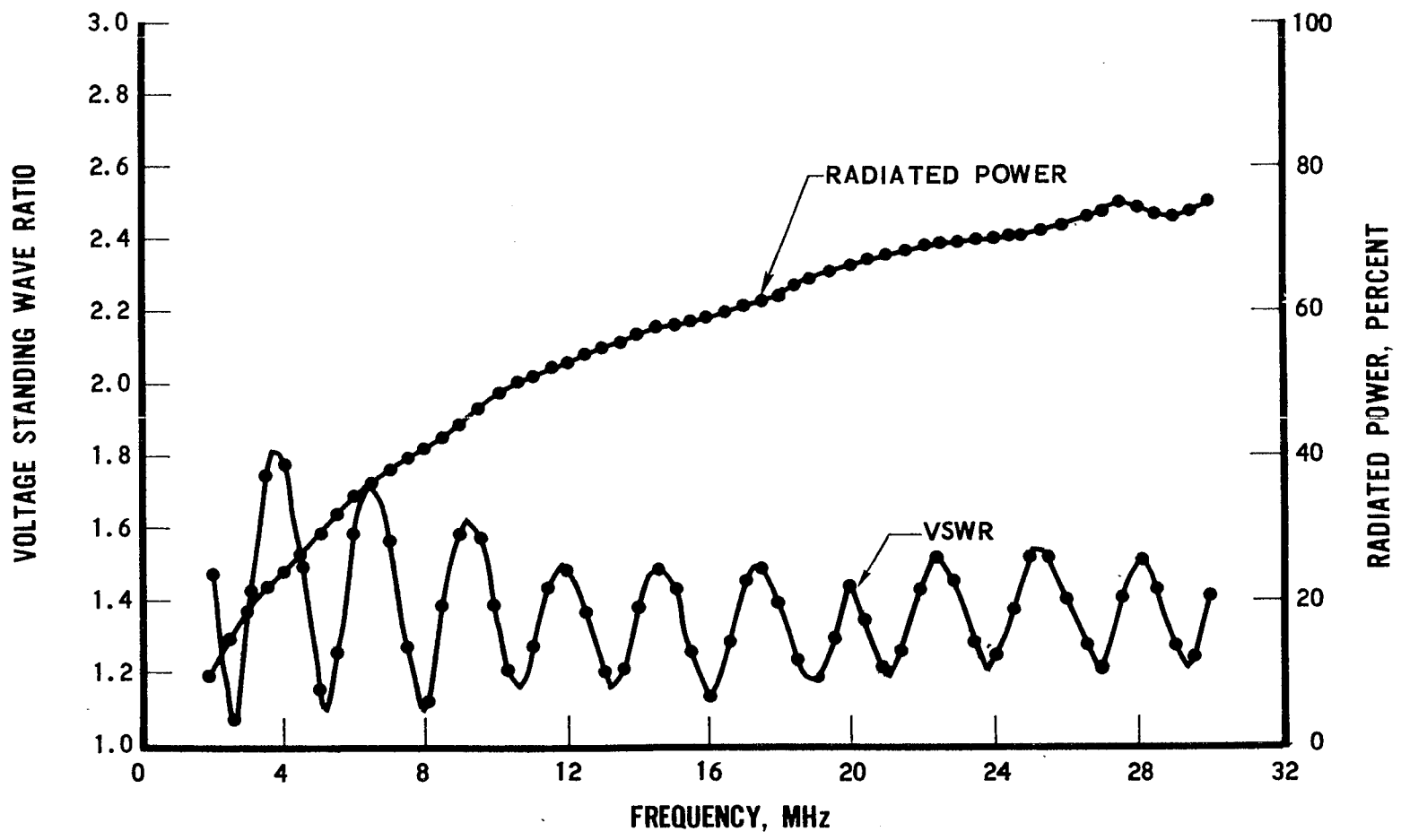Fig. 7. Input Reactance vs Frequency

Fig. 8. Reflected and Radiated Power vs Frequency

The electric fields within and just beyond the working volume are shown in Figs. 9 through 11. In Fig. 9 the ideal line is one in which the vertical electric field is 1 volt divided by the separation distance between plates. It can be seen that within the working volume the vertical electric field is very nearly ideal, and it is only beyond the working volume that the field drops off at the higher frequencies. In Fig. 10 the discontinuity in E_z is due to the charge density on the plate. Actually E_z reverses direction when $z > 6\,m$, but this does not show up on a plot of absolute field strength. Fig. 11 shows the vertical electric field plotted as a function of y.

Radiation field patterns are shown in Figs. 12 and 13. On the $y = 0$ plane the electric field vector is linearly polarized, since $E\phi = 0$ from symmetry. In both Figs. 12 and 13, the 0° and 180° directions correspond to viewing the simulator from the top and bottom plates respectively, while the 90° and 270° directions correspond to viewing the simulator from the source end and the load end respectively. It can be seen that the simulator is tending to be an end-fire antenna at the higher frequency.
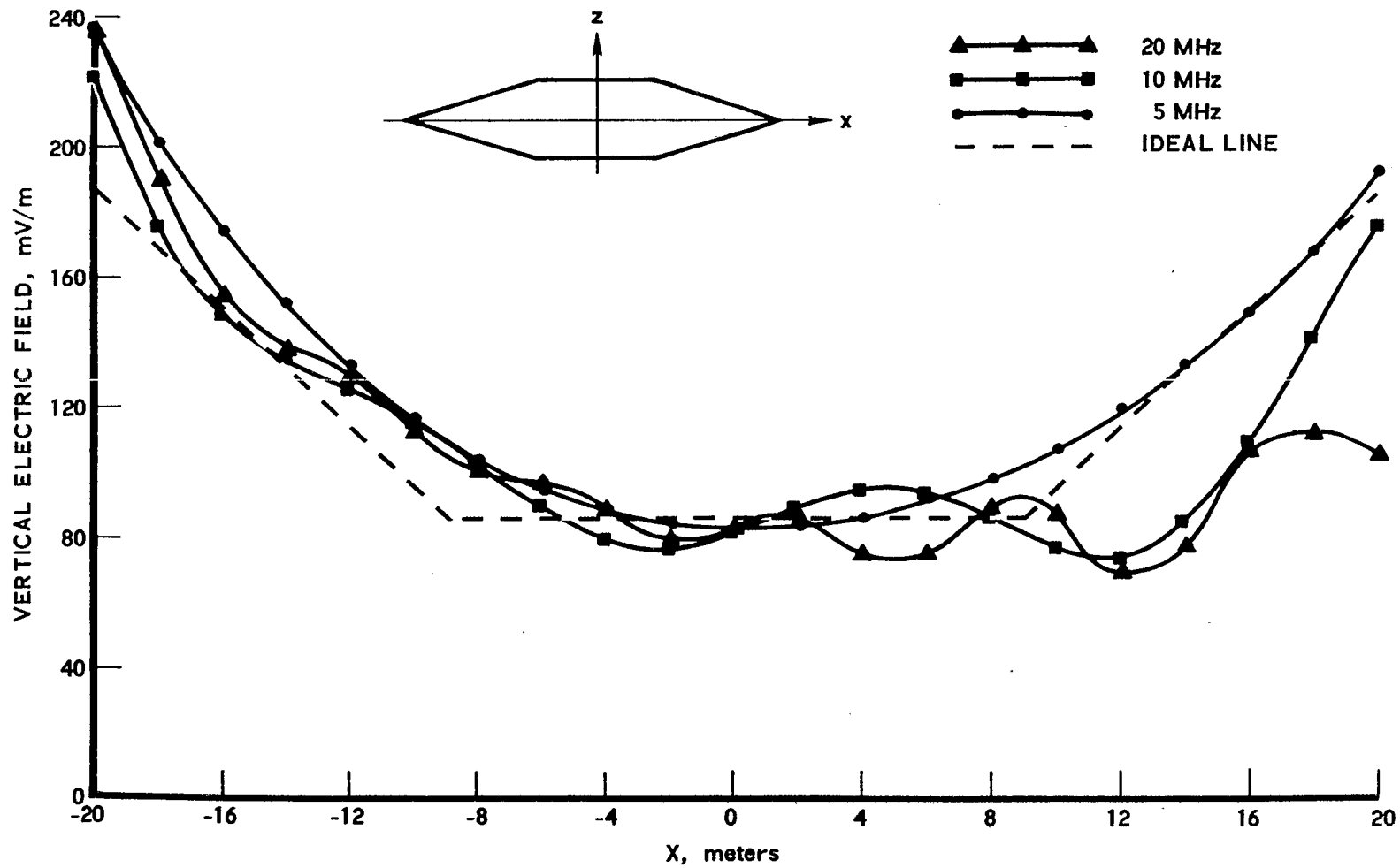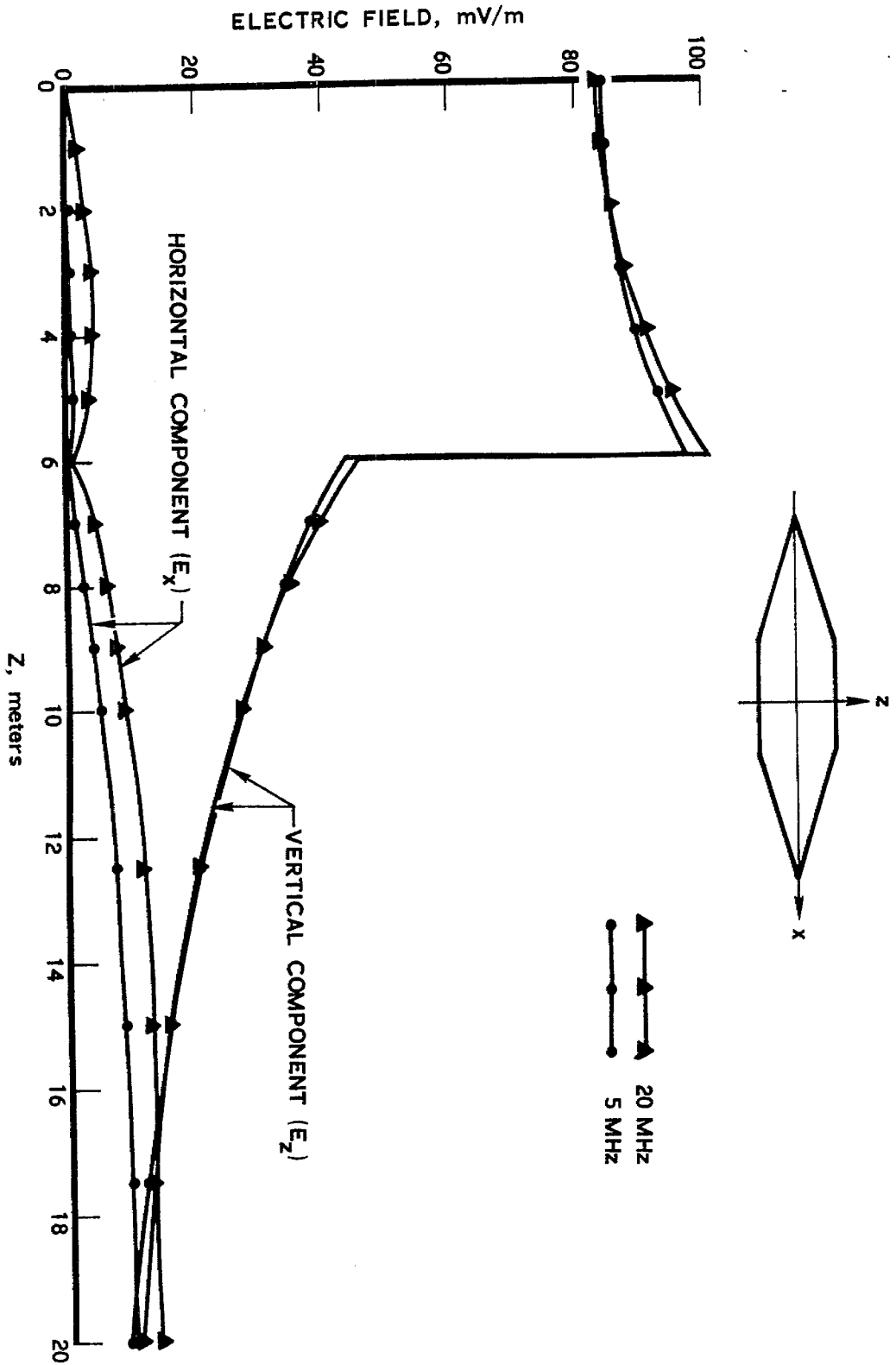
20

Fig. 9. Electric Field Distribution at y = 0, z = 0

ELECTRIC FIELD, mV/m

HORIZONTAL COMPONENT (E_x)

VERTICAL COMPONENT (E_z)

Z, meters

20 MHz

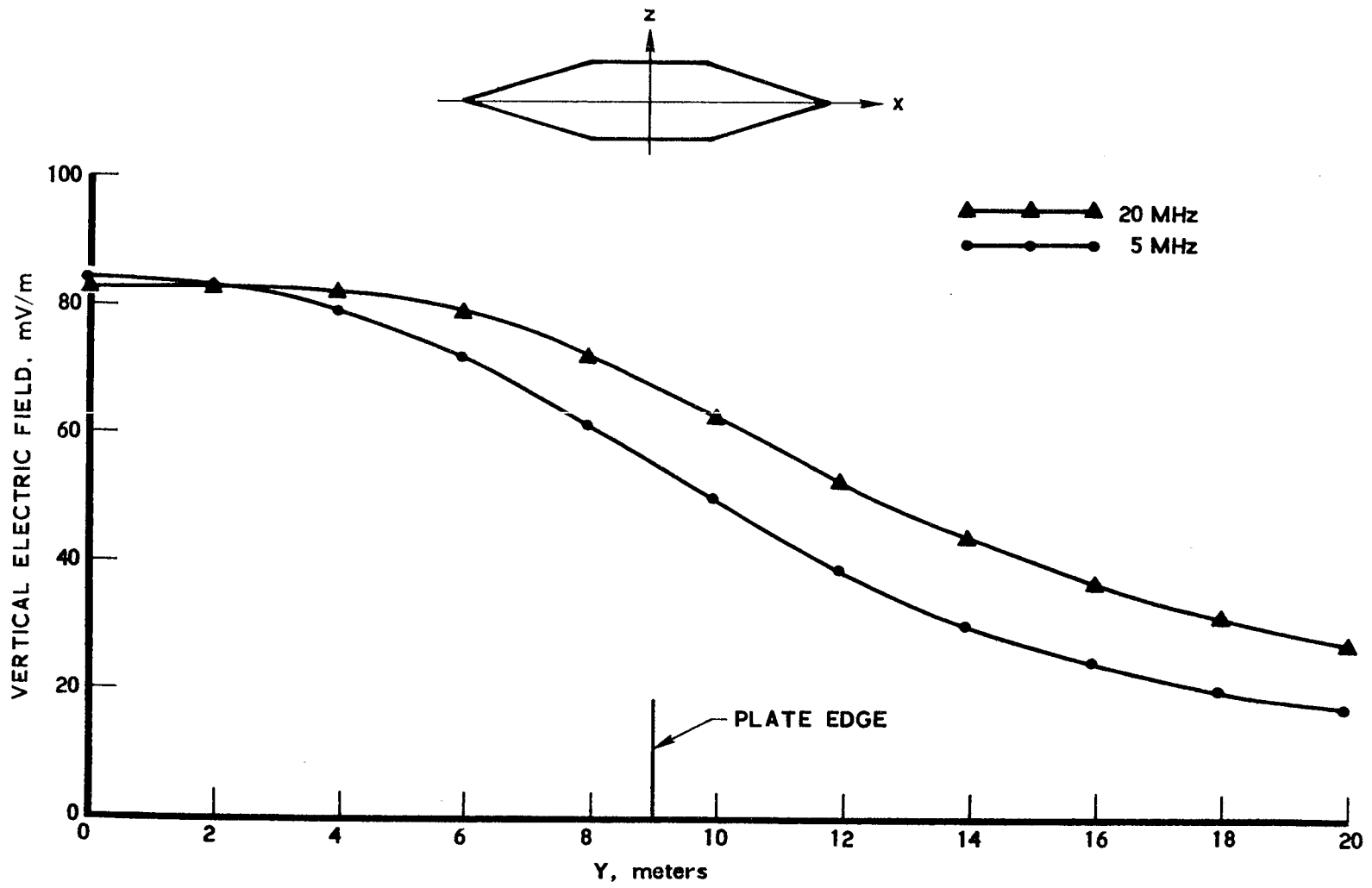5 MHz

Fig. 10. Electric Field Distribution at x = 0, y = 0
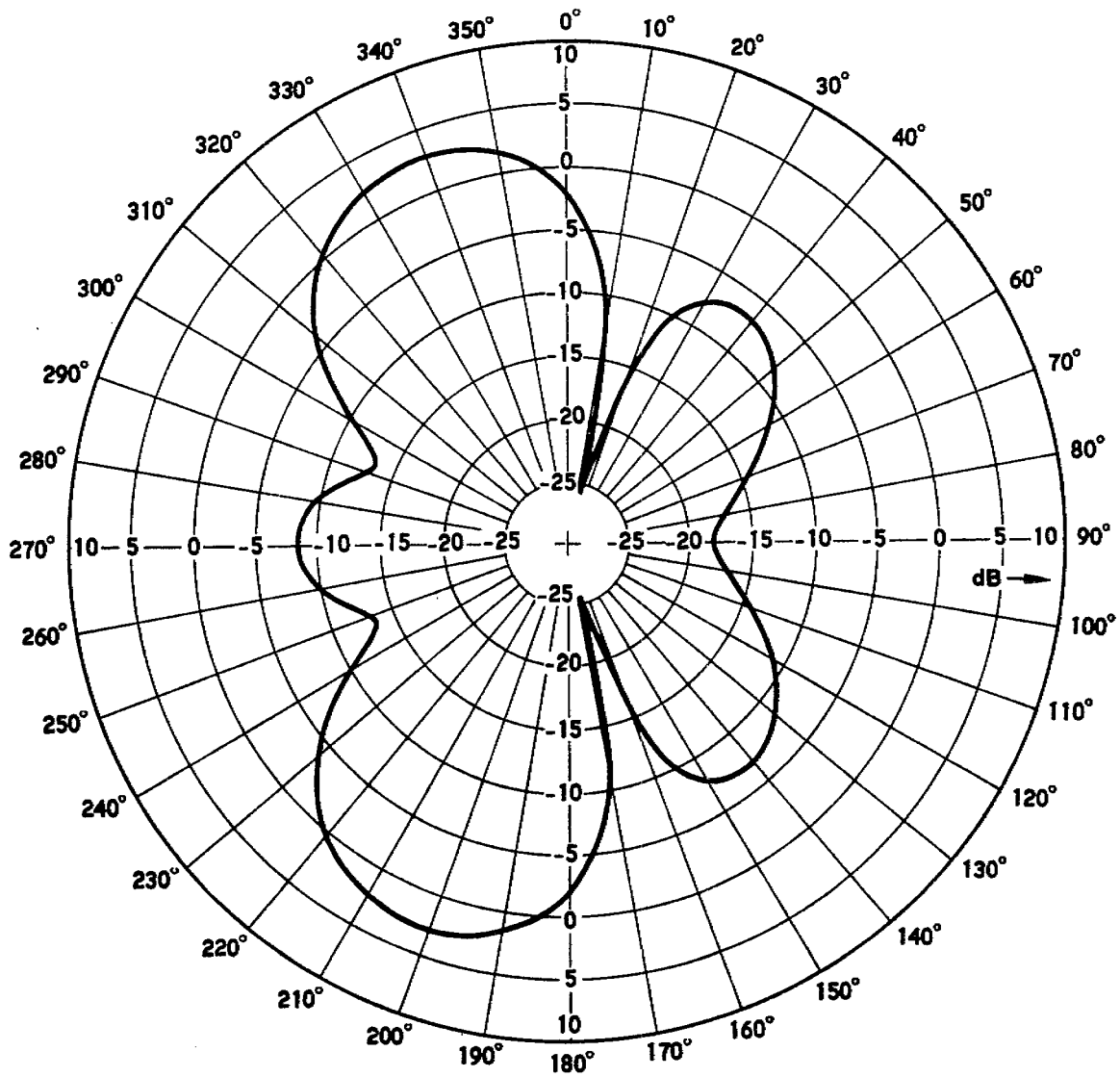
Fig. 11. Vertical Electric Field at x = 0, z = 0

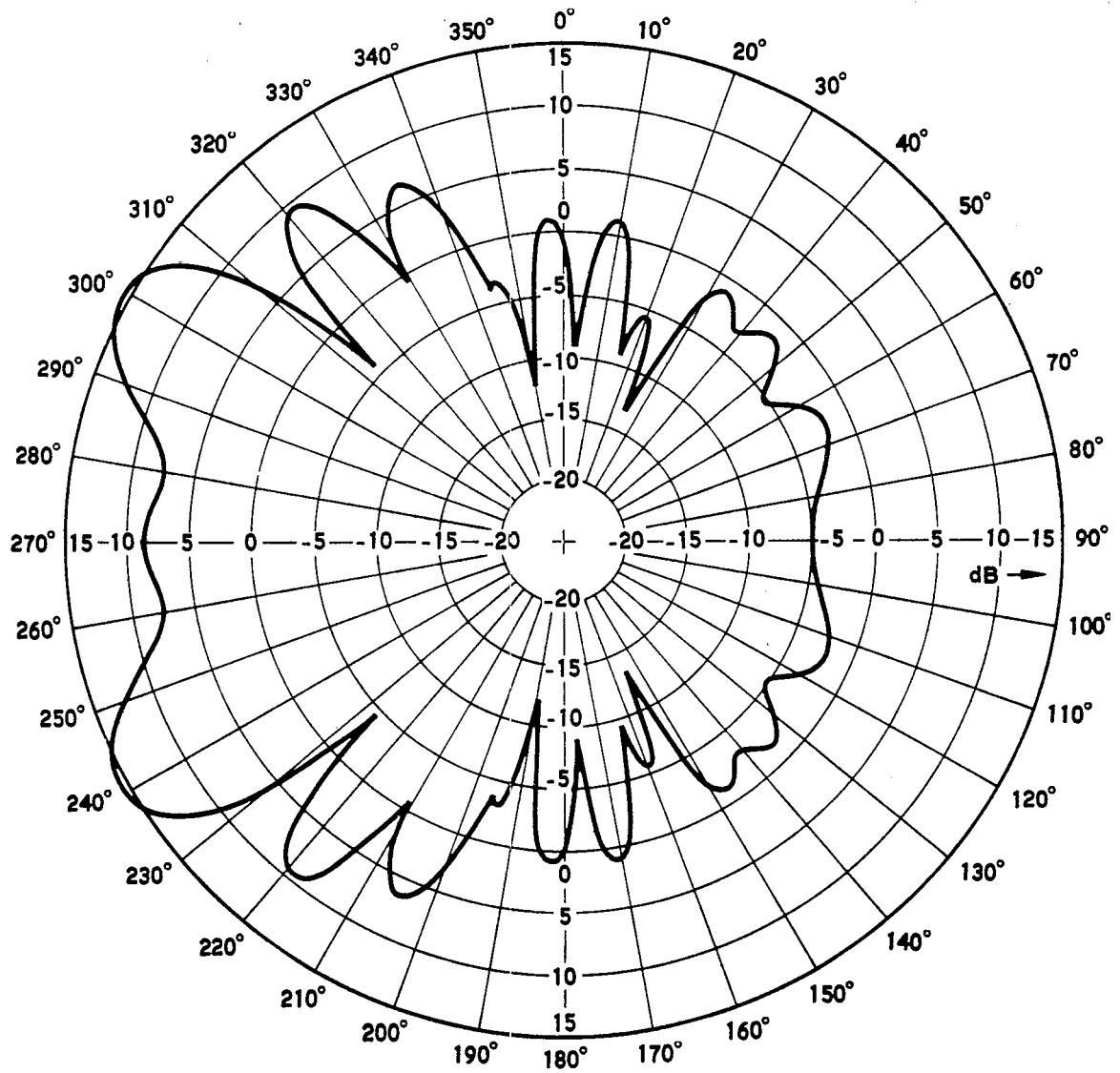Fig. 12. Radiation Pattern at 6 MHz (y = 0 plane)

Fig. 13. Radiation Pattern at 26 MHz (y = 0 plane)

V. CONCLUSIONS AND DISCUSSION

The transmission line simulator is apparently an efficient radiator at the higher frequencies. The radiation pattern resembles that of an end-fire, or traveling wave, antenna. The radiation, however, appears to be taking place beyond the working volume of the simulator; a large contribution may come from the discontinuity between the end of the working volume and the beginning of the tapered section. Inside most of the working volume, the electric field was reasonably uniform and quite close to its ideal value. Furthermore, the power lost due to reflections was low. It can be concluded, therefore, that this geometry appears acceptable from the standpoint of EMP simulation.

No attempt was made at optimizing the selected design, although it is obvious that the present computer program could be extremely useful for this purpose. Finally, some remarks should be made about the extension of the calculations to higher frequencies. For the calculation at 30 MHz the arc length L was divided into 100 subsections (N = 100), and the calculation required slightly less than 3 minutes on the CDC 7600 computer. The computer time increases faster than N^2 because of the required integrations over y and y'. Therefore, even though there is sufficient storage capacity to handle factors of 4 or 5 increase in frequency, which requires N to be increased by the same factor, such a calculation may be undesirable from the standpoint of cost.

REFERENCES

1. C. E. Baum, "Impedances and Field Distributions for Parallel Plate Transmission Line Simulators," *Sensor and Simulation Notes*, Vol. 1, No. 21, June 1966; (also see: T. L. Brown and K. D. Granzow, "A Parameter Study of Two Parallel Plate Transmission Line Simulators of EMP Sensor and Simulation Note 21," *Sensors and Simulation Notes*, Vol. 3, No. 52, April 1968).

2. R. F. Harrington, *Field Computation by Moment Methods*, The Macmillan Company, New York (1968).

3. R. H. Ott, "The Scattering by a Two-Dimensional Periodic Array of Plates," Technical Report 2148-2, The Ohio State University Research Foundation, Antenna Laboratory, Columbus, Ohio (30 June 1966).

4. R. Mittra, W. A. Davis, and D. V. Jamnejad, "An Integral Equation for Plane Wave Scattering by Thin Plates," presented at 1972 Fall Meeting of the International Scientific Radio Union, Williamsburg, Virginia, 12-15 December 1972.

5. J. R. Mautz and R. F. Harrington, "Radiation and Scattering from Bodies of Revolution," *Appl. Sci. Res.* 20 (6), 405 (June 1969).

6. D. S. Jones, *The Theory of Electromagnetism*, The Macmillan Company, New York (1964), Chap. 9.

7. G. H. Brown and O. M. Woodward, Jr., "Experimentally Determined Radiation Characteristics of Conical and Triangular Antennas," *RCA Rev.* 13 (4), 425 (December 1952).

APPENDIX

The parametric equations which describe S can be derived from Fig. 1. First, the total arc length L can be expressed in terms of the dimensions of the simulator as follows:

$$L = 2 \left[G + D + \sqrt{4R^2 + (H - G)^2} \right] \qquad \text{(A-1)}$$

Next let

$$\alpha_x = \frac{4R}{L - 2(G + D)} \qquad \text{(A-2)}$$

$$\alpha_z = \frac{2(H - G)}{L - 2(G + D)} \qquad \text{(A-3)}$$

$$\alpha_W = \frac{4(W_H - W_G)}{L - 2(G + D)} \qquad \text{(A-4)}$$

Then $x(t)$, $z(t)$, $W(t)$, and $\vec{u}_t(t)$ are given as follows:

$$\left. \begin{array}{l} x = -\left(R + \dfrac{D}{2} \right) \\[2ex] z = t \\[2ex] W = W_G \\[2ex] \vec{u}_t = \vec{u}_z \end{array} \right\} \quad 0 \leq t < \frac{G}{2} \qquad \text{(A-5)}$$

$$\left. \begin{array}{l} x = -\left(R + \dfrac{D}{2} \right) + \alpha_x \left(t - \dfrac{G}{2} \right) \\[2ex] z = \dfrac{G}{2} + \alpha_z \left(t - \dfrac{G}{2} \right) \\[2ex] W = W_G + \alpha_W \left(t - \dfrac{G}{2} \right) \\[2ex] \vec{u}_t = \alpha_x \vec{u}_x + \alpha_z \vec{u}_z \end{array} \right\} \quad \frac{G}{2} \leq t < \frac{L}{4} - \frac{D}{2} \qquad \text{(A-6)}$$

28

$$x = t - \frac{L}{4}$$

$$\dot{z} = \frac{H}{2}$$

$$W = W_H \left. \right\} \quad \frac{L}{4} - \frac{D}{2} \leq t < \frac{L}{4} + \frac{D}{2} \qquad \text{(A-7)}$$

$$\vec{u}_t = \vec{u}_x$$

$$x = \frac{D}{2} + \alpha_x \left(t - \frac{L}{4} - \frac{D}{2} \right)$$

$$z = \frac{H}{2} - \alpha_z \left(t - \frac{L}{4} - \frac{D}{2} \right)$$

$$W = W_H - \alpha_W \left(t - \frac{L}{4} - \frac{D}{2} \right) \left. \right\} \quad \frac{L}{4} + \frac{D}{2} \leq t < \frac{L}{2} - \frac{G}{2} \qquad \text{(A-8)}$$

$$\vec{u}_t = \alpha_x \vec{u}_x - \alpha_z \vec{u}_z$$

$$x = R + \frac{D}{2}$$

$$z = \frac{L}{2} - t \left. \right\} \quad \frac{L}{2} - \frac{G}{2} \leq t \leq \frac{L}{2} \qquad \text{(A-9)}$$

$$W = W_G$$

$$\vec{u}_t = -\vec{u}_z$$

where $\vec{u}_x$ and $\vec{u}_z$ are unit vectors in the x and z directions respectively.
Finally, the expressions for $L/2 \leq t \leq L$ may be generated from Eqs. (A-5)
through (A-9), since from symmetry

$$x \left(t - \frac{L}{2} \right) = x(t) \qquad \text{(A-10)}$$

$$z \left(t - \frac{L}{2} \right) = -z(t) \qquad \text{(A-11)}$$

$$W\left(t - \frac{L}{2}\right) = W(t) \qquad\qquad \text{(A-12)}$$

$$\vec{u}_x \cdot \vec{u}_t\left(t - \frac{L}{2}\right) = -\vec{u}_x \cdot \vec{u}_t(t) \qquad\qquad \text{(A-13)}$$

$$\vec{u}_z \cdot \vec{u}_t\left(t - \frac{L}{2}\right) = \vec{u}_z \cdot \vec{u}_t(t) \qquad\qquad \text{(A-14)}$$